Design of a Solar Thermoelectric Generator

Undergraduate Honors Thesis
Presented in Partial Fulfillment of the Requirements for Graduation with Distinction
at The Ohio State University

By: Sarah Watzman

The Ohio State University
Department of Mechanical and Aerospace Engineering
Submitted April 4th, 2013

Defense Committee:
Professor Joseph Heremans, Advisor
Professor Sandip Mazumder

Abstract

In a world where fossil fuels dominate as energy sources, the need for an economically and commercially viable renewable energy source is dire. The processes through which fossil fuels are formed do not occur fast enough to replenish their sources to meet society's demands, and combustion of fossil fuels produces carbon dioxide, a greenhouse gas linked to global warming. Solar energy has proven itself to be a promising alternative, with the field dominated by photovoltaics on the consumer-scale and solar thermal power on the plant-scale. Yet solar thermal systems have an innate advantage in their use of all wavelengths of incident radiation as opposed to just light. In this research, thermoelectrics are being explored as a viable option for small-scale solar thermal applications. Thermoelectrics are based on the Seebeck effect, stating that a voltage is induced when a temperature gradient is applied to the junctions of two differing materials; in the case of a solar thermoelectric generator (STEG), the hot side is the solar absorber and the cold side is the heat sink. This research proposes to design, build, and test a prototype STEG to contribute to the further development of STEGs as reasonable solar thermal energy sources for the consumer market. The design process involved calculating and optimizing the energy balance across the absorber, minimizing heat losses, analyzing heat transfer through the thermoelectric elements, and analyzing the electrical power system. The testing process involved assembling the system, measuring the balance of heat and heat losses, and measuring the electrical power generated by the thermoelectric module connected to varying resistive loads in order to ultimately measure the STEG's efficiency. Literature suggests that STEGs can reach 5.2% efficiency when operating in a vacuum and 0.03% in air, both without optical

concentration, although this STEG only reached a peak efficiency of approximately 0.03%.

Acknowledgements

I would like to thank Dr. Joseph Heremans for his support and guidance as my advisor throughout the duration of this research project. I would also like to thank Dr. Robert Siston for encouraging me to get involved in undergraduate research. I would like to thank the graduate students in the Thermal Nanomaterials Lab as well as the student workers in the machine shop for all of their help and advice. I would also like to thank Trio Glass for donating the low-emissivity glass used for the chamber covering. Last but definitely not least, I would like to thank my family and friends for their support and encouragement throughout this project.

Table of Contents

List of Figures

List of Tables

Nomenclature

A_{abs}	area of the absorber (m^2)
A_n	cross-sectional area of one n-type element (m^2)
A_p	cross-sectional area of one p-type element (m^2)
A_{TE}	cross-sectional area of a thermoelectric element, consisting of one n-type and one p-type element (m^2)
α	solar absorptance of absorber
C_{opt}	optical concentration ratio
ε	combined emittance (0.05)
ε_e	effective emittance between bottom of absorber and cold-side of thermoelectric module
ε_s	emmitance of top surface of absorber
I	current through generator (A)
k_n	thermal conductivity of n-type bismuth telluride thermoelectric material $\left(1.4\ \frac{W}{mK}\right)$
k_p	thermal conductivity of p-type bismuth telluride thermoelectric material $\left(1.2\ \frac{W}{mK}\right)$
κ	thermal conductance of bismuth telluride thermoelectric module $\left(4.888\ \frac{W}{K}\right)$
q_i	heat flux coming into STEG from sun $\left(\frac{W}{m^2}\right)$
Q_{abs}	heat transferred to absorber (W)
Q_{comv}	heat lost due to convection (W)
$Q_{rad,bottom}$	heat lost due to radiation from the bottom of the absorber (W)
$Q_{rad,top}$	heat lost due to radiation from the top of the absorber (W)
Q_{TE}	heat transferred through thermoelectric elements
R_L	load resistance (Ω)
R_S	source resistance from thermoelectric module (Ω)
ρ_n	resistivity of n-type bismuth telluride thermoelectric material (27 μΩ-m)
ρ_p	resistivity of p-type bismuth telluride thermoelectric material (21 μΩ-m)
S_n	Seebeck coefficient for n-type bismuth telluride thermoelectric material$\left(-230\frac{\mu V}{K}\right)$
S_p	Seebeck coefficient for p-type bismuth telluride thermoelectric material $\left(225\frac{\mu V}{K}\right)$
S_{tot}	Total Seebeck coefficient for bismuth telluride thermoelectric module $\left(46.6\ \frac{mV}{K}\right)$
σ	Stefan-Boltzmann constant $\left(5.67 \times 10^{-8}\ \frac{W}{m^2K^4}\right)$
P_{out}	output power (W)
P_{sun}	input power from sun (W)
T_{amb}	ambient temperature (294 K)
T_c	cold side (heat sink) temperature (294K)
T_h	hot side (absorber) temperature (473K)

τ	transmittance of glass covering
V_{OC}	open circuit voltage (V)
V_{out}	output voltage across load on STEG (V)
ZT	non-dimensional thermoelectric figure of merit

Introduction

Motivation

Because fossil fuels such as coal, oil, and natural gas are the most predominately used energy sources, an intense need exists for an economically and commercially viable renewable energy source [1]. Although these fossil fuels account for around 88% of the world's energy needs, the rate at which they are produced is significantly lower than the rate at which society is using them. Furthermore, the combustion of fossil fuels produces carbon dioxide – the number one greenhouse gas – making the use of fossil fuels the leading cause of global warming [1]. Thus, many alternative, renewable energy sources have been proposed. One feasible solution is solar energy, with the field dominated by photovoltaics and solar thermal power [2]. Nevertheless, photovoltaic cells utilize only a small portion of radiation emitted by the sun – visible light -- yet the entire spectrum of solar radiation may be converted into heat [3]. Through the use of thermoelectric devices, this heat is then converted into electricity. Therefore, solar thermal systems have an innate advantage in their use of all wavelengths of incident radiation. Solar thermal energy, through the use of thermoelectrics, is also advantageous because it involves direct energy conversion from heat into electricity, eliminating the need for intermediate steps to obtain a usable output [4].

Although recognized as the renewable energy field with the highest potential, solar thermal power has been slower to develop technologically and in a consumer market until recently [5]. Currently, solar thermal energy has only been widely implemented in large-scale power plants with concentrators, while photovoltaics dominate the renewables market for household electricity generation [2]. On a large-

scale, Rankine cycle engines are powered by solar thermal energy [5]; but for small-scale solar thermal applications, thermoelectrics are more efficient [2]. This research proposes to design, build, and test a small-scale solar thermoelectric generator (STEG) to contribute to the further development of STEGs as a reasonable solar thermal energy source in a consumer market.

Semiconductors

Semiconductors are materials that conduct electricity when electrons are energized to breach an energy gap; but in comparison to conductors, semiconductors have a smaller number of electrons available to do so. If an electron is excited from a valence band or an impurity level to a conduction band across an energy gap, a positive hole is left in its place and conduction is caused by electron excitation into the conduction band – these types of materials have an effectively negative charge and are consequently called n-type materials. Conversely, if the energy gap is large and an impurity state exists between the valence band and the conduction band, excited electrons may jump from the valence band to an orbital around the impurity atom. In this case, the mobile hole left in the valence band is the cause for conduction, forcing the material to have an effectively positive charge and therefore be called a p-type material [6].

Furthermore, when a semiconductor is placed inside a temperature gradient, the material's lattice experiences lattice waves, or phonons, flowing through it from the hot side to the cold side. Because the lattice interacts with the electrons responsible for conduction, some of these electrons are pulled through the lattice with the phonon wave,

resulting in the phonon drag effect. This effect is a source of thermoelectricity, although diffusion of electrons dominates at room temperature [6].

Thermoelectric Theory

The direct conversion of a temperature difference into electricity can be explained by the Seebeck effect, which states that a voltage is induced when a temperature gradient is applied to the junctions of two differing materials [6]. Figure 1 illustrates this concept in an open thermoelectric circuit. For STEGs, the materials are n-type and p-type thermoelectric materials, the junctions are the substrate for the thermoelectric module, $T + \Delta T$ represents the absorber temperature, T represents the heat sink temperature, and the voltage difference is measured across a load or open circuit.

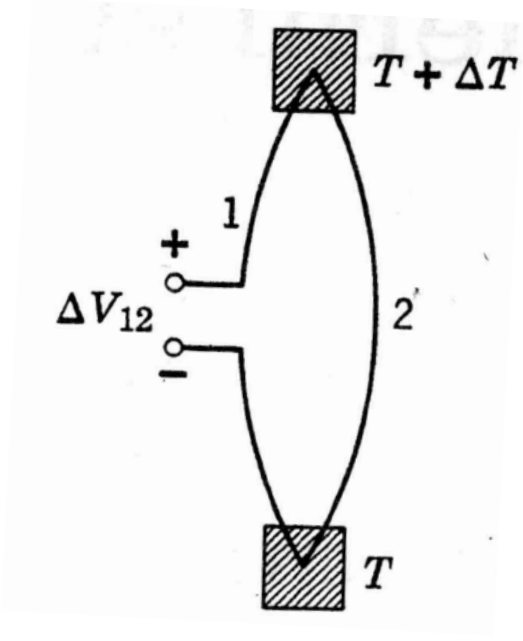

Figure 1: Open Thermoelectric Circuit [6]

The induced voltage, ΔV_{12}, is proportional to ΔT by the difference in the Seebeck coefficients of the two materials, as shown through the following equation. The Seebeck

coefficients are considered to be material properties and are assumed to be constant at all temperatures used in this experiment [6].

$$\Delta V_{12} = (S_1 - S_2)\Delta T$$

Similarly, the Peltier Effect describes the inverse of this behavior – when an electrical current is passed through the junction of two differing materials, heat is either lost or absorbed at the junction according to the direction of the current [6]. The Peltier coefficient, π, demonstrates the proportionality between the heat flowing from a material due to a current and the current itself; this is illustrated in Figure 2.

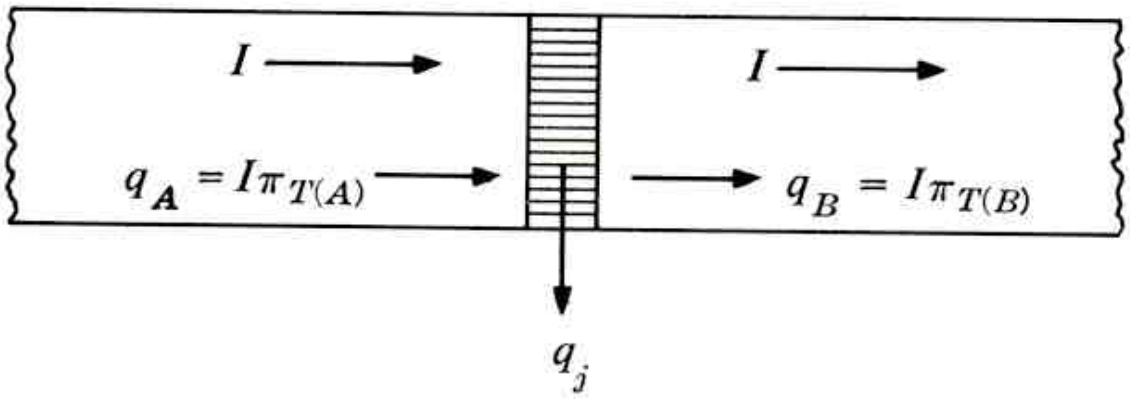

Figure 2: Current Flow through Dissimilar Materials [4]

The Seebeck coefficient and the Peltier coefficient are related through the following Kelvin relation [6]:

$$\pi = TS$$

Both the Seebeck Effect and the Peltier Effect are functions of material state, but these effects are only seen when two differing materials are connected. Additionally, these effects are distinct from Joule heating, which is present in any semiconductor with a current flowing through it [6].

Thermoelectric Modules

In a typical thermoelectric module, alternating n-type and p-type thermoelectric elements are connected by substrates, electrically in series and thermally in parallel. Heat is absorbed through the top substrate and flows through the thermoelectric elements; it is then rejected at the bottom substrate. Loads can be attached to the module's external electrical connection [7]. This device set-up is shown in Figure 3.

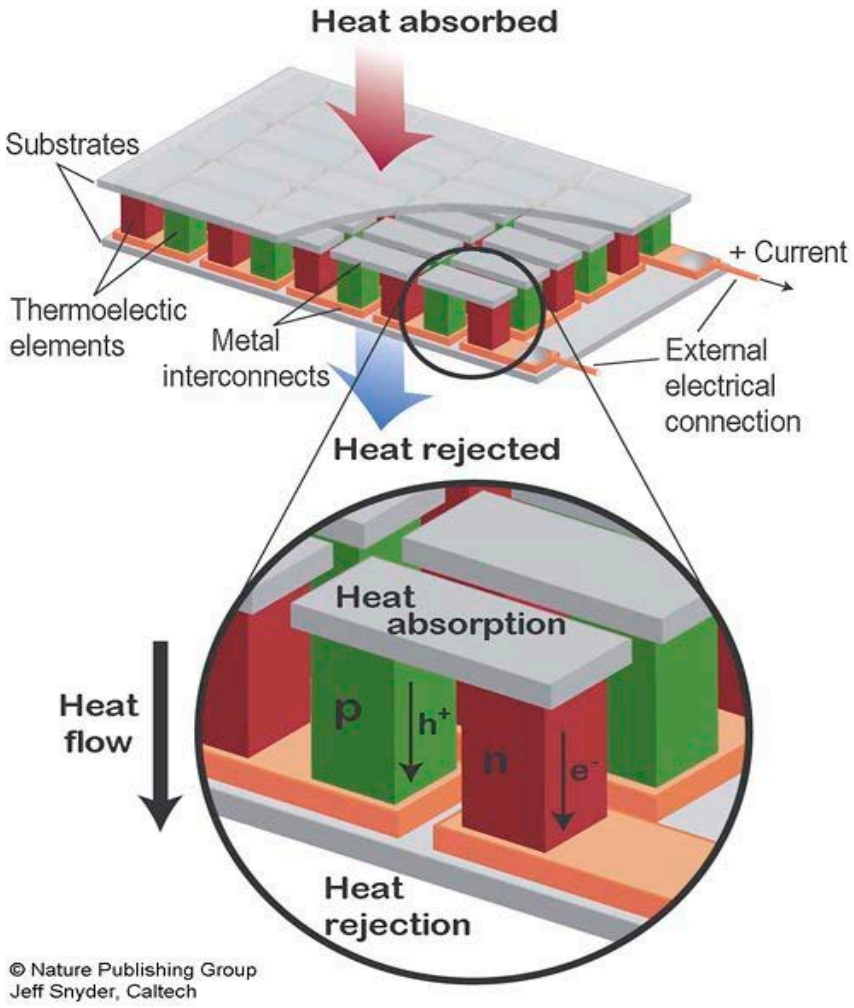

Figure 3: Thermoelectric Materials in a Thermoelectric Module [7]

Previous Work

Maria Telkes was one of the first people to utilize zinc-antimony thermoelectric materials in solar generators, calculating their efficiency in STEGs to be much higher than the commonly available alloys of her time [8]. Using a flat-plate collector with two glass panes covering it and zinc-antimony alloys combined with negative bismuth alloys as thermoelectric materials, STEG efficiency reached 0.63% and was calculated to reach 1.05% if four panes of glass were to have been applied to the same device. When optical concentration was applied to this system, the efficiency increased to 3.35%. In comparison, only 0.068% efficiency was reached with chromel p-constantan thermoelectric materials in the flat-panel, two pane system [9].

H. J. Goldsmid observed that, although metals and metal alloys have a high ratio of electrical to thermal conductivity, they have low thermoelectric power; yet semiconductors have a large enough thermoelectric power to compensate for their lower ratio of conductivities [10]. Thus, he applied this concept to the use of bismuth telluride semiconductors as thermoelectric materials in a STEG. He first built and tested a STEG with a flat plate absorber at low operating temperature, resulting in an overall efficiency under 1%. Trying again with a STEG equipped to operate at higher temperatures and utilizing a collector, Goldsmid again achieved lower efficiencies than expected (still under 1%). Nevertheless, he noted that higher efficiencies are definitely possible if higher temperatures are achieved, one method of which is through the use of solar collectors [11].

Gang Chen's work has served to increase STEG efficiency using thermal concentration as opposed to optical concentration, eliminating the requirement for

expensive equipment to track the sun in order to attain the necessary optical concentration to significantly increase the efficiency. Using a flat-panel solar absorber, solar radiation is collected, converted into heat, and concentrated onto the thermoelectric module; this heat flow is shown in Figure 4. Through the use of bismuth telluride thermoelectric materials and an evacuated system to eliminate convective heat losses, Chen has achieved efficiencies of 4.6% - 5.2% in the system shown in Figure 5 [2]. The research presented in this paper is modeled from Chen's work.

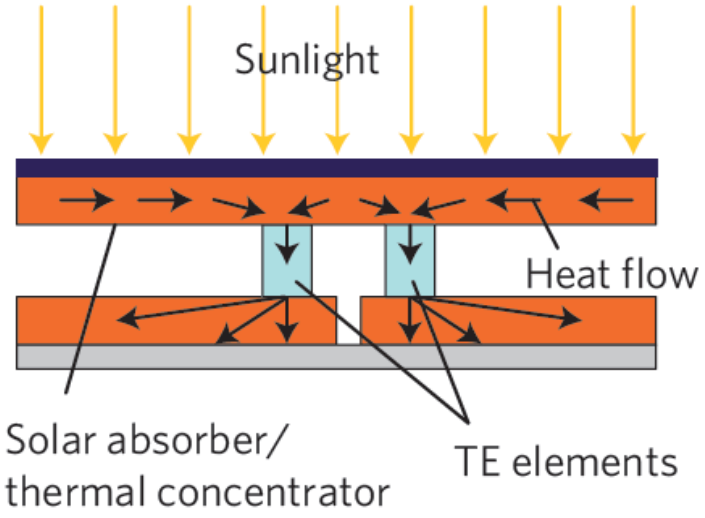

Figure 4: Heat Flow through Cross-Section of STEG [2]

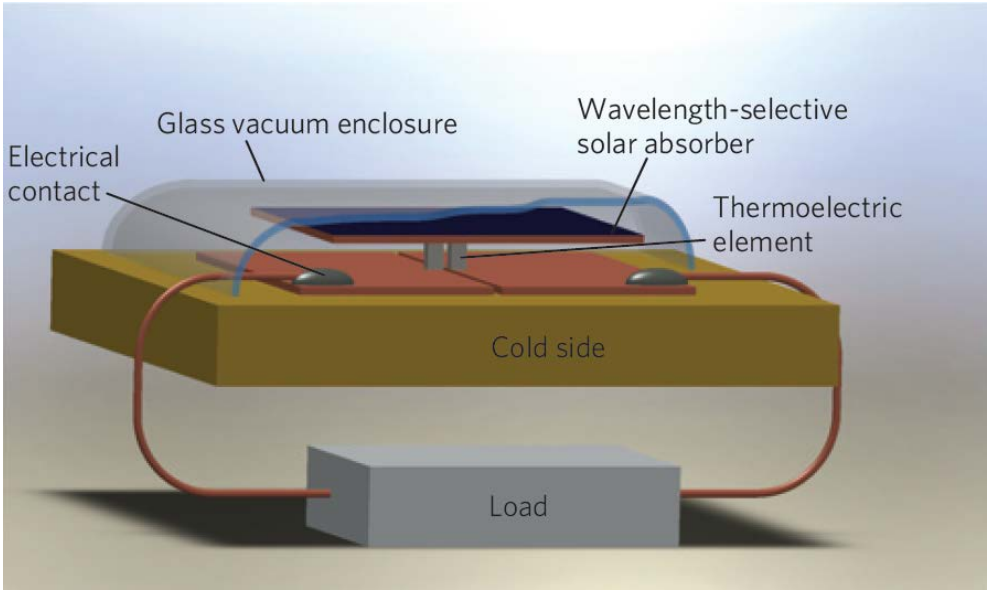

Figure 5: Evacuated STEG with Flat-Panel Solar Absorber [2]

Experimental Procedures

Theoretical Analysis

The generator can be modeled using the electrical schematic shown in Figure 6, where the open circuit voltage and the source resistance represent the STEG and the load is a resistor with the output as the voltage drop across this resistor.

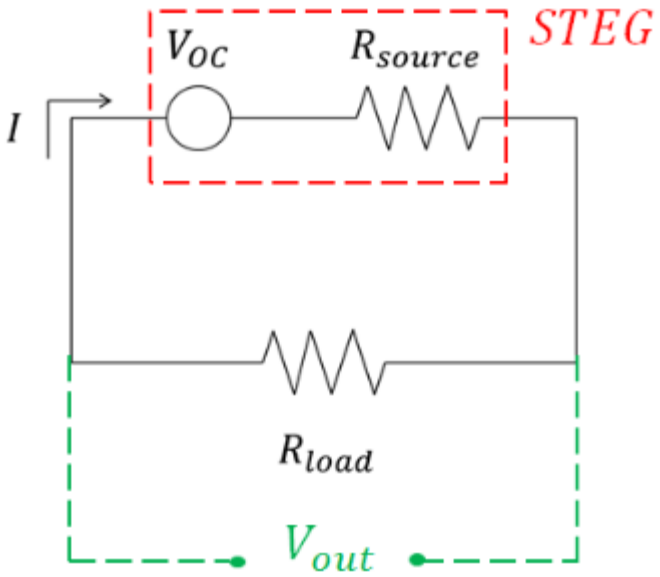

Figure 6: Electrical System Schematic

The open circuit voltage is equal to the current multiplied by the sum of the resistances [12]:

$$V_{OC} = I(R_S + R_L)$$

For maximum power output, the load resistance must equal the source resistance, so the current can be represented as [4]:

$$I = \frac{V_{OC}}{2R_S}$$

Seebeck's relation states that the voltage induced by a temperature gradient is proportional to the temperature gradient, with the proportionality constant being represented by the difference in the Seebeck coefficients of the p-type and n-type materials [4]:

$$V_{OC} = (S_p - S_n)(T_h - T_c)$$

Furthermore, the resistance of a thermoelectric module is given by the following equation [4]:

$$R_S = \rho_p \frac{l}{A_p} + \rho_n \frac{l}{A_p}$$

Assuming the cross-sectional areas of the p-type and n-type thermoelectric elements are the same, these areas can be represented as half of the total thermoelectric area for one module, reducing the source resistance to:

$$R_S = \frac{2l}{A_{TE}}(\rho_p + \rho_n)$$

Combining the previous equations for current, open circuit voltage, and source resistance, the current becomes:

$$I = \frac{A_{TE}(S_p - S_n)(T_h - T_c)}{4l(\rho_p + \rho_n)}$$

The rate of heat transferred to the thermoelectric module from the absorber is described by the following equation [13]:

$$Q_{TE} = -k_p A_p \left(\frac{dT_p}{dx}\right)_{x=0} - k_n A_n \left(\frac{dT_n}{dx}\right)_{x=0} + IT_h(S_p - S_n)$$

With the location of $x = 0$ being the top (hot side) of the thermoelectric elements in the module and $x = l$ being the bottom (cold side) of the thermoelectric elements, and assuming linearity across the short length of the thermoelectric module, the derivatives are expressed as:

$$\left(\frac{dT_p}{dx}\right)_{x=0} = \left(\frac{dT_n}{dx}\right)_{x=0} = \frac{T_h - T_c}{0 - l} = \frac{T_c - T_h}{l}$$

Substituting these expressions and the previous expression for current back into the expression for the total heat transfer yields:

$$Q_{TE} = \frac{A_{TE}}{2}\left(\frac{T_h - T_c}{l}\right)(k_p + k_n) + \frac{A_{TE}(S_p - S_n)^2(T_h - T_c)T_h}{4l(\rho_p + \rho_n)}$$

The energy balance across the absorber can be expressed in terms of the solar radiation incident on the top of the absorber, the heat leaving the bottom of the absorber to the thermoelectric module, the heat losses due to radiation from the top and bottom of the absorber, and the heat losses due to convection [13]:

$$Q_{abs} = Q_{TE} + Q_{rad,bottom} + Q_{rad,top} + Q_{conv}$$

Because this STEG is designed for an evacuated environment, the convective heat losses are zero (although the system was later determined to not be able to hold a vacuum, as described further in this paper). An illustration of the absorber's energy balance can be seen in Figure 7.

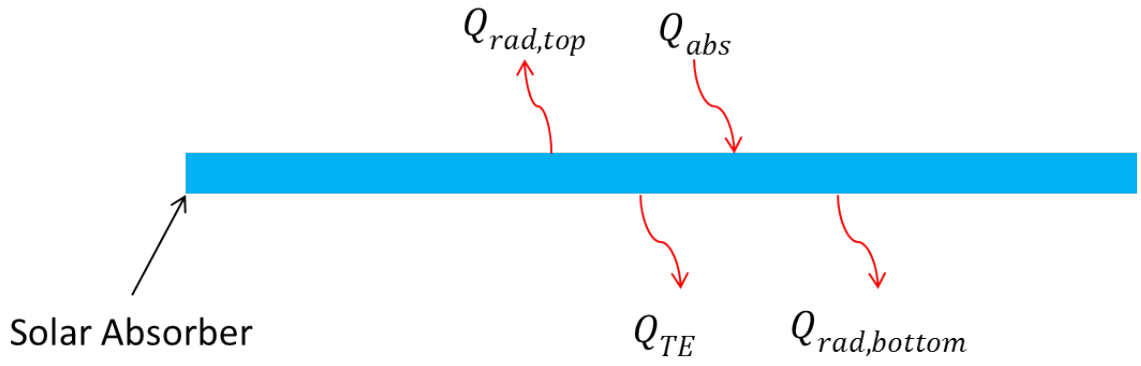

Figure 7: Energy Balance across Solar Absorber

The radiation incident on the top of the absorber is expressed as the product of the transmittance of the glass covering, the solar absorptance of the absorber, the optical concentration ratio of the system, the heat flux from the sun incident on the system, and the absorber area [13]:

$$Q_{abs} = \tau\alpha C_{opt} q_i A_{abs}$$

The heat losses from the bottom and top of the absorber due to radiation are expressed as [13]:

$$Q_{rad,bottom} = A_{abs}\varepsilon_e\sigma(T_h^4 - T_c^4)$$

$$Q_{rad,top} = A_{abs}\varepsilon_s\sigma(T_h^4 - T_{amb}^4)$$

The combined emittance of the top surface of the absorber and the bottom of the absorber is equal to the sum of the individual emittances. Assuming $T_c = T_{amb}$, the sum of the heat losses due to radiation is represented by [13]:

$$Q_{rad,bottom} + Q_{rad,top} = A_{abs}\varepsilon\sigma(T_h^4 - T_c^4)$$

Therefore the energy balance across the absorber is described by:

$$\tau\alpha C_{opt} q_i A_{abs}$$

$$= \frac{A_{TE}}{2}\left(\frac{T_h - T_c}{l}\right)\left(k_p + k_n\right) + \frac{A_{TE}\left(S_p - S_n\right)^2 (T_h - T_c)T_h}{4l\left(\rho_p + \rho_n\right)} + A_{abs}\varepsilon\sigma(T_h^4 - T_c^4)$$

With no optical concentration, $C_{opt} = 1$; τ and α can also be assumed to be 1 [13]. Thus, the ratio of the absorber area to the thermoelectric area is given by:

$$\frac{A_{abs}}{A_{TE}} = \frac{\left(\frac{T_h - T_c}{2l}\right)\left(k_p + k_n\right) + \frac{\left(S_p - S_n\right)^2 (T_h - T_c)T_h}{4l\left(\rho_p + \rho_n\right)}}{q_i - \varepsilon\sigma(T_h^4 - T_c^4)}$$

Using typical values of T_h, T_c, l, q_i, and ε [2], values of k_p, k_n, S_p, S_n, ρ_p, ρ_n for bismuth telluride thermoelectric materials [14], the ratio was determined to be approximately 246:1. This roughly means that for a square foot size absorber, one thermoelectric module is necessary. With this design, 100 W of solar power is to give approximately 179°C of temperature gradient across the thermoelectric module (estimating the ambient/cold side temperature to be 21°C and the hot side temperature to be 200°C, which is within the temperature range of optimal performance for bismuth telluride materials [2]).

Hardware Design

A Tellurex G2-35-0315 thermoelectric module, using bismuth telluride thermoelectric material, is used as the thermoelectric module for this STEG and can be seen in Figure 8.

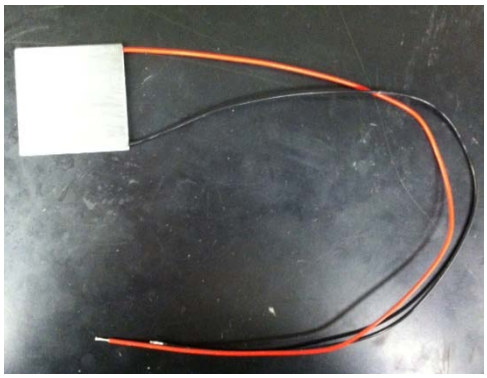

Figure 8: Thermoelectric Module

The module is connected to the bottom of a 3/16 inches thick, 11.5 inches x 11.5 inches square aluminum plate, which is used as the absorber. The absorber dimensions were determined from the ratio of the absorber area to the ratio of the thermoelectric area using the conditions listed in the previous section. This size was determined using the

properties of a different model module which broke in the building process – the ideal size for the model used would have been 12.64 inches x 12.64 inches, but the same absorber was used due to time and material constraints. The top of the aluminum plate is coated with Thurmalox Solar Coating, and the bottom of the plate was sanded to smooth the surface in order to obtain a high reflectivity and minimal emissivity. The bottom of the absorber with the module attached can be seen in Figure 9.

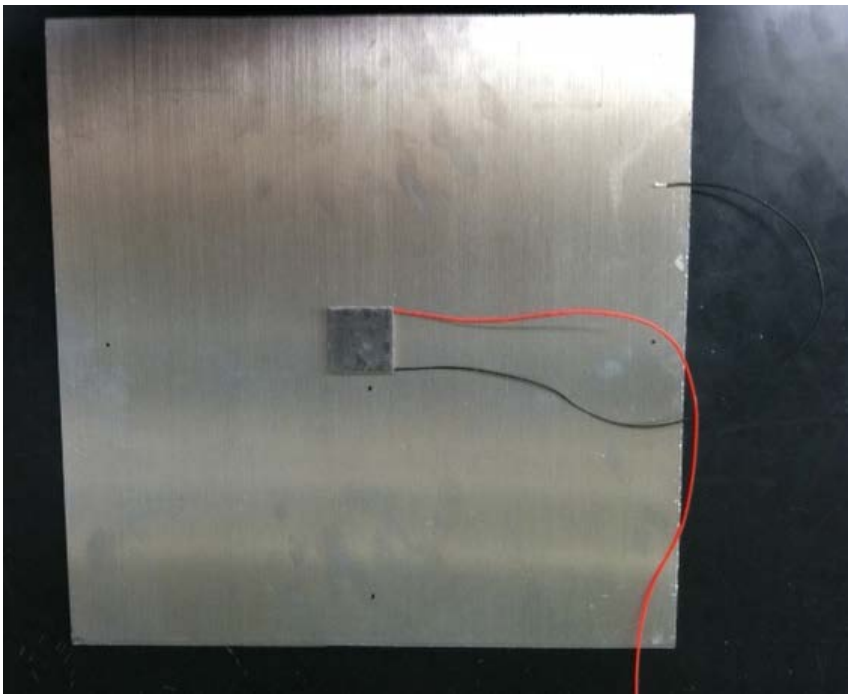

Figure 9: Bottom of Absorber with Module

The STEG's heat sink is made from a 1 foot square, 5/8 inches thick aluminum plate. A National Pipe Thread tapered hole is tapped into the heat sink for the hose fitting to connect the system to a vacuum pump (the hole was initially tapped in the wrong direction and consequently filled with brass, as seen in the picture). The outside edges of the heat sink were originally lined with rubber to avoid glass-to-metal contact under a vacuum since the system's covering is made of glass. The absorber (with the module attached) is connected to the heat sink. The heat sink alone is shown in Figure 10.

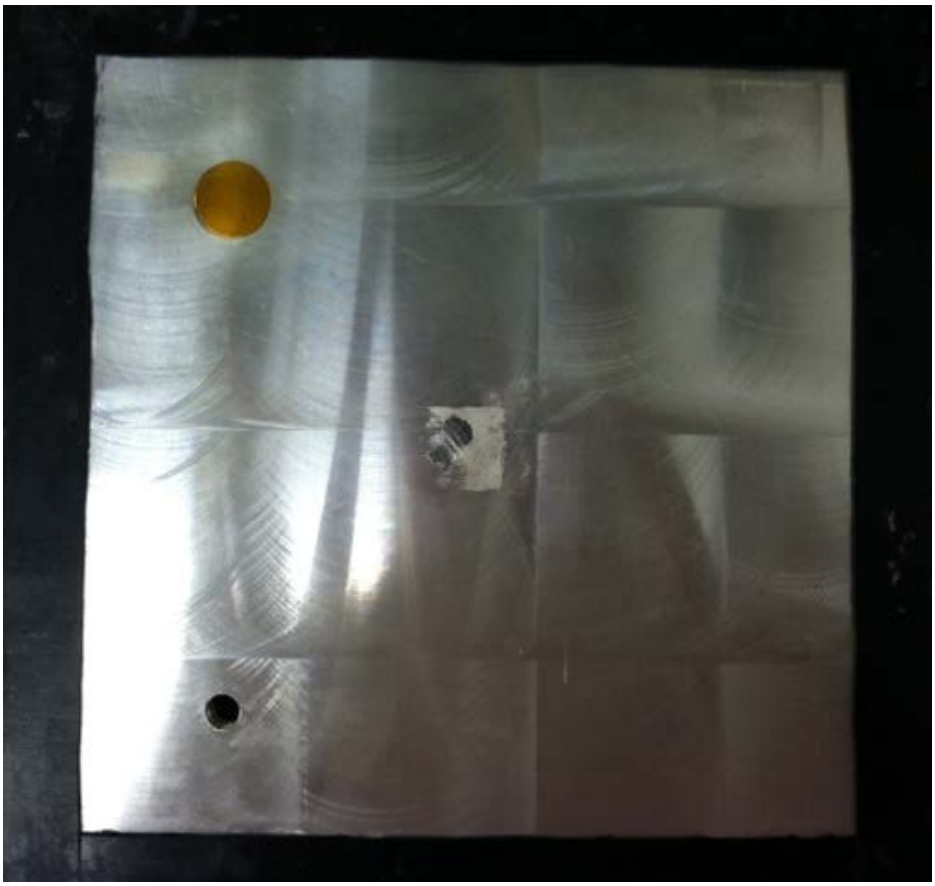

Figure 10: Heat Sink

The STEG's covering is comprised of low-emissivity window glass, which allows light to enter the glass but keeps the heat in the system [15]. The sealant used to hold the covering together is a heat resistant RTV silicon sealant. The glass covering can be seen in Figure 11.

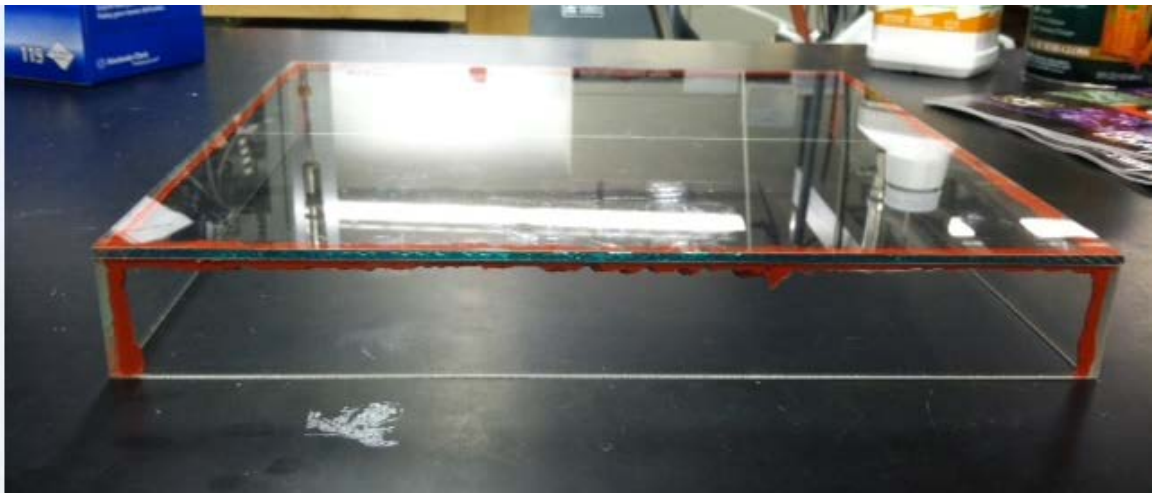

Figure 11: Vacuum Covering with Low-Emissivity Glass

Testing of Device

Before the absorber and thermoelectric module were attached to the heat sink, the chamber was tested to ensure that it was airtight. Once an airtight seal was achieved, the system began to be evacuated, but the glass covering could not maintain the pressure differential and ultimately imploded, as seen in Figure 12. Thus, the evacuation method was abandoned, introducing convective heat losses into the system which were not originally taken into account for the design. In an effort to reduce these convective heat losses as much as possible without an evacuated environment, foam insulation was added between the solar absorber and the heat sink (measured thermal conductance of 0.04 W/m/K). Additionally, a new glass covering was built and used due to the glass's capability to keep the heat inside the system from the low-emissivity coating [15].

Figure 12: Imploded Chamber after Partial Evacuation

In order to determine the source resistance of the thermoelectric module to load match, the system's AC resistance was measured in an open circuit and determined to be 3.45 Ω. The thermal conductivity was found to be 1.37 W/m/K when averaging directional thermal conductivities [14], leading to a thermal conductance of 4.89 W/K using the dimensional properties of the module. Using the open circuit voltage versus hot side temperature curve for the module (shown in Figure 13) and determining the slope over the STEG's operating temperature range, the total Seebeck coefficient of the module was determined to be 46.6 mV/K.

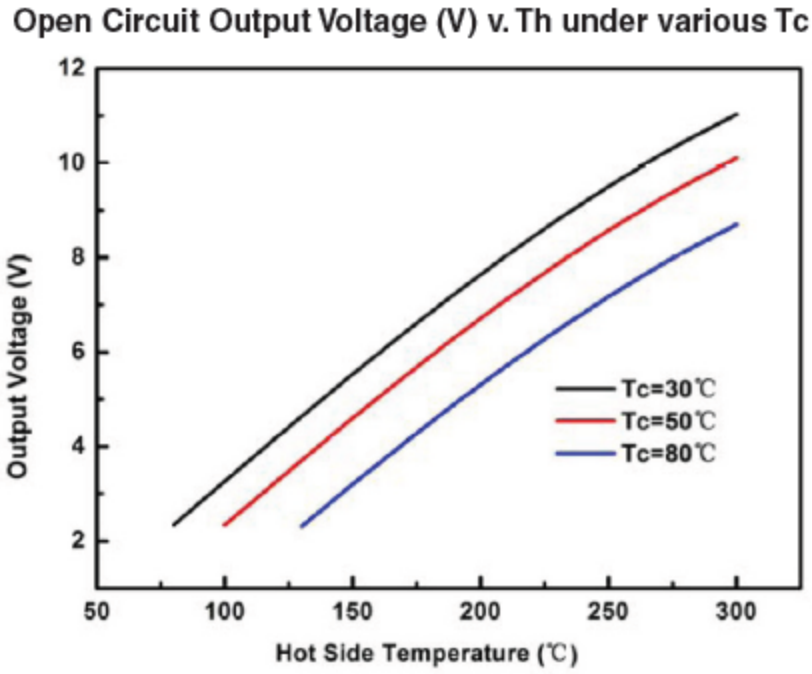

Figure 13: Performance Curve for Thermoelectric Module [16]

Open Circuit Test (Indoors)

The first test of the STEG was an open circuit test in the lab under an overhead light, connecting the module output wires to a DC voltmeter. With the glass covering removed and the light above the testing area turned off, the absorber was covered with foil until the voltage reading reached approximately 0 V. Next, the foil was quickly removed, the glass covering placed onto the STEG, and the light in the testing area turned on. The open circuit voltage was recorded for given time intervals until steady-state was reached. The constant input solar power was recorded using a solar power meter, made by Ambient Weather, and determined to be 2.6 W/m^2, or 0.222 W. This experimental set-up can be seen in Figure 14.

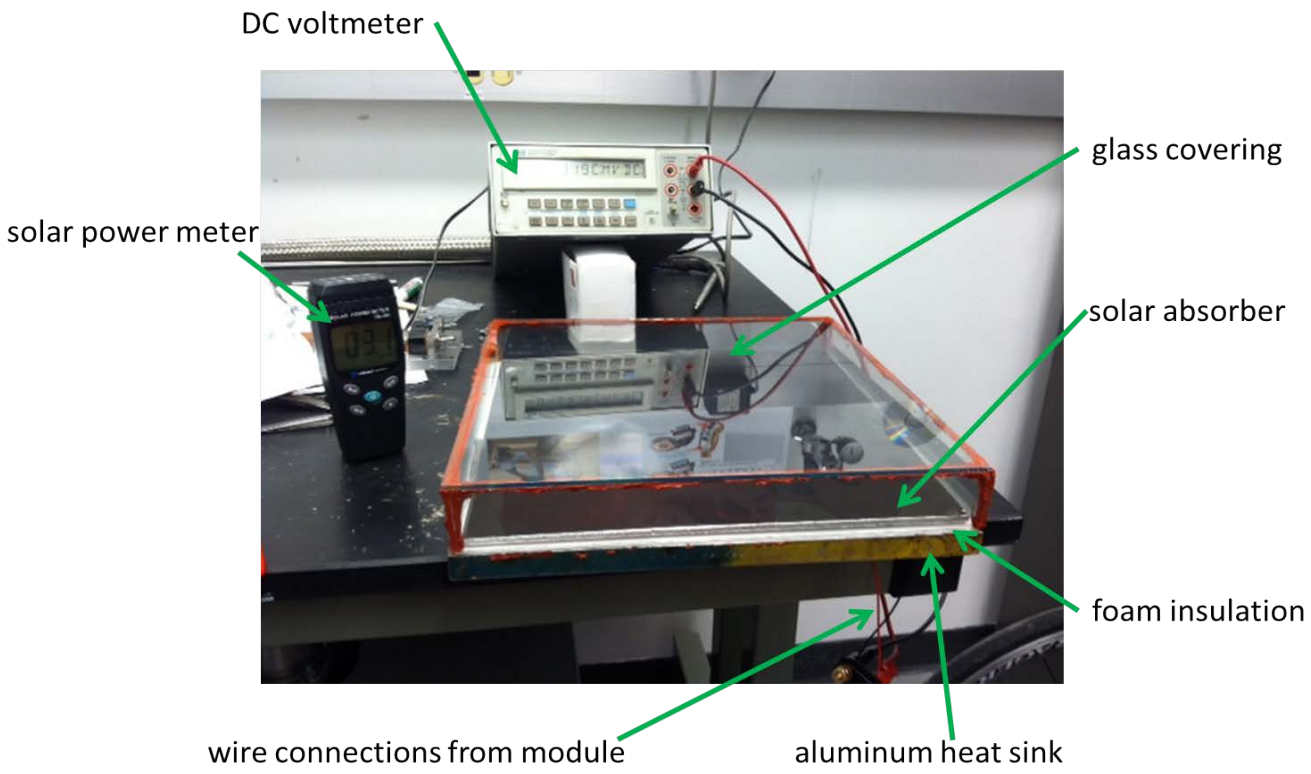

Figure 14: Inside Test Setup

Loaded Tests (Outdoors)

For the outside test of the STEG, the device was first placed in a shaded area for about an hour to allow the entire device to reach ambient temperature. When the STEG was moved into the sun, the solar power input and open circuit voltage were measured every minute until the STEG reached steady-state. Once steady-state was reached, a decade box was connected to the output wires of the module as the resistive load, and a DC voltmeter was connected across the load. Increasing the load from 0 Ω to 110 Ω (the max of the decade box), the output voltage was recorded at each interval of resistance. This test was repeated in another location (since the sun had moved) with the same procedure, except the resistive load was started at 110 Ω and was decreased to 0 Ω. The experimental setup can be seen in Figure 15.

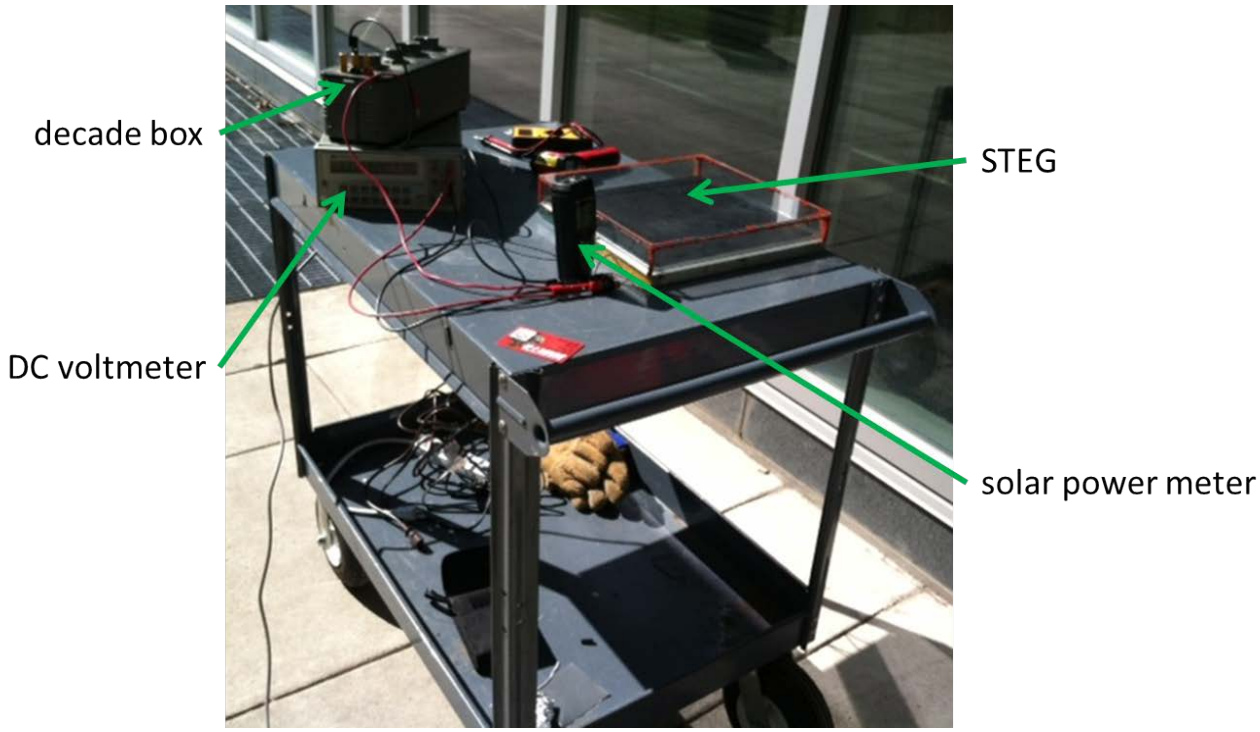

Figure 15: Outside Test Setup

Results

Open Circuit Test (Indoors)

The steady-state open circuit voltage for the STEG was determined to be about 4.54 mV reached in about 80 minutes, as shown in Figure 16. This open circuit voltage was not maintained by the STEG, though – once the peak voltage was reached, the open circuit voltage began to decrease (although Figure 16 only shows data up to steady-state).

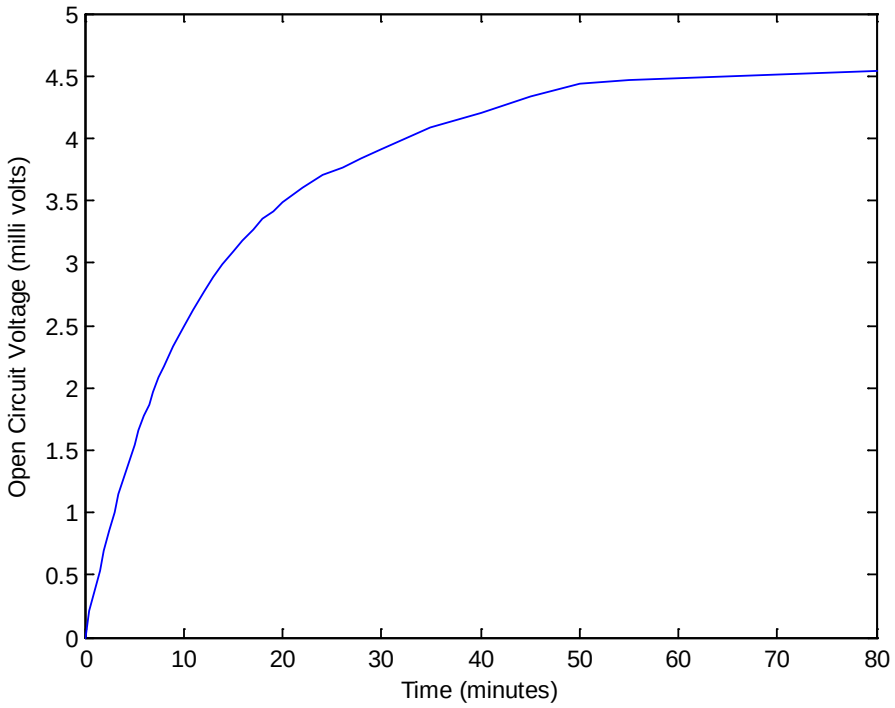

Figure 16: Open Circuit Voltage Results for Indoor Test

Loaded Tests (Outdoors)

For the first test outdoors, the STEG reached a steady-state open circuit voltage of 0.660 V in approximately 60 minutes. The input solar flux was measured at 834 W/m^2, the maximum output power was 0.0209 W, and the peak system efficiency was 0.0293%. For the second loaded test, the input solar flux was measured at 750 W/m^2, the maximum power output was 0.0191 W, and the peak system efficiency was 0.0299%. These results are summarized in Table 1.

Table 1: Loaded Test Results for Outdoor Tests

	Loaded Test 1	Loaded Test 2
Input Solar Flux (W/m^2)	834	750
Input Solar Power (W)	71.16	63.99
Open Circuit Voltage (V)	0.660	0.640
Maximum Power Output (W)	0.0209	0.0191
Heat Losses (W)	71.14	63.97
Peak Module Efficiency	0.0302%	0.0285%
Peak System Efficiency	0.0293%	0.0299%

The input power from the sun was calculated by multiplying the measured solar flux incident on the absorber with the absorber area [3]. The output power of the STEG was calculated by dividing the output voltage squared by the load resistance [12]. The current through the STEG was calculated by dividing the output voltage by the load resistance [12]. These equations can be seen below.

$$P_{sun} = q_i A_{abs}$$

$$P_{out} = \frac{V_{out}^2}{R_L}$$

$$I = \frac{V_{out}}{R_L}$$

Using the open circuit voltage from each loaded test along with the thermal conductance and total Seebeck coefficient of the bismuth telluride thermoelectric module, the heat transferred through the module was calculated. Then, the efficiencies of the module and of the entire system were calculated [4]. These equations are as follows (not that the equation for the heat transferred through the thermoelectric module is an approximation, neglecting the Peltier heat):

$$Q_{TE} = \kappa \frac{V_{OC}}{S_{tot}}$$

$$\eta_{mod} = \frac{P_{out}}{Q_{TE}}$$

$$\eta_{sys} = \frac{P_{out}}{P_{sun}}$$

The output voltage versus load resistance curves are shown in Figure 17 for the first loaded test and in Figure 18 for the second loaded test. As demonstrated in the graphs, the output voltage initially increases quickly as load resistance increases then levels off to more slowly approach the steady-state open circuit voltage values for both tests.

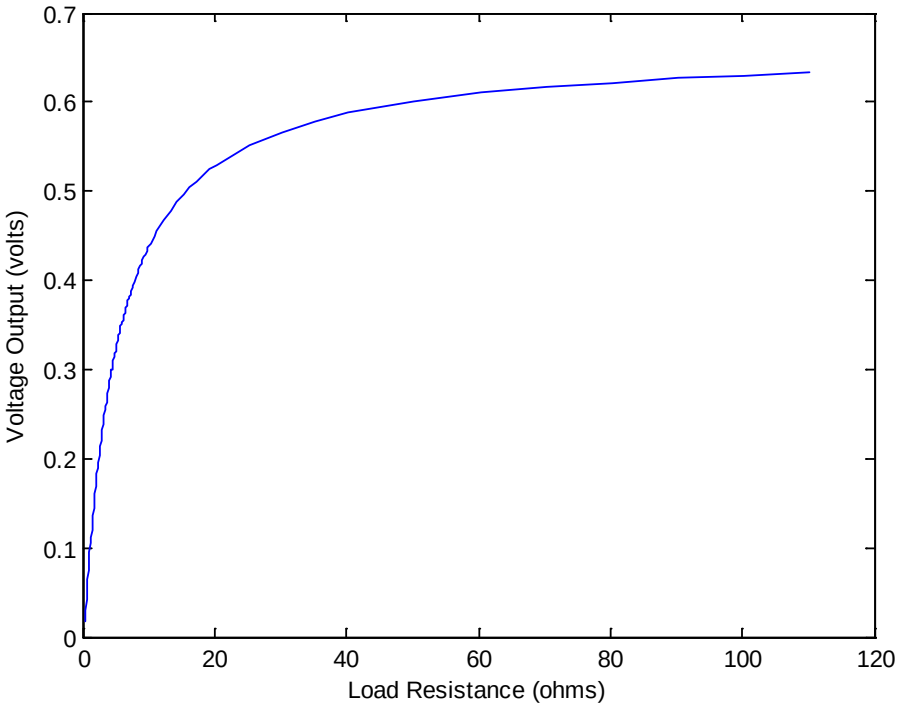

Figure 17: Voltage Output vs. Load Resistance for Loaded Test 1

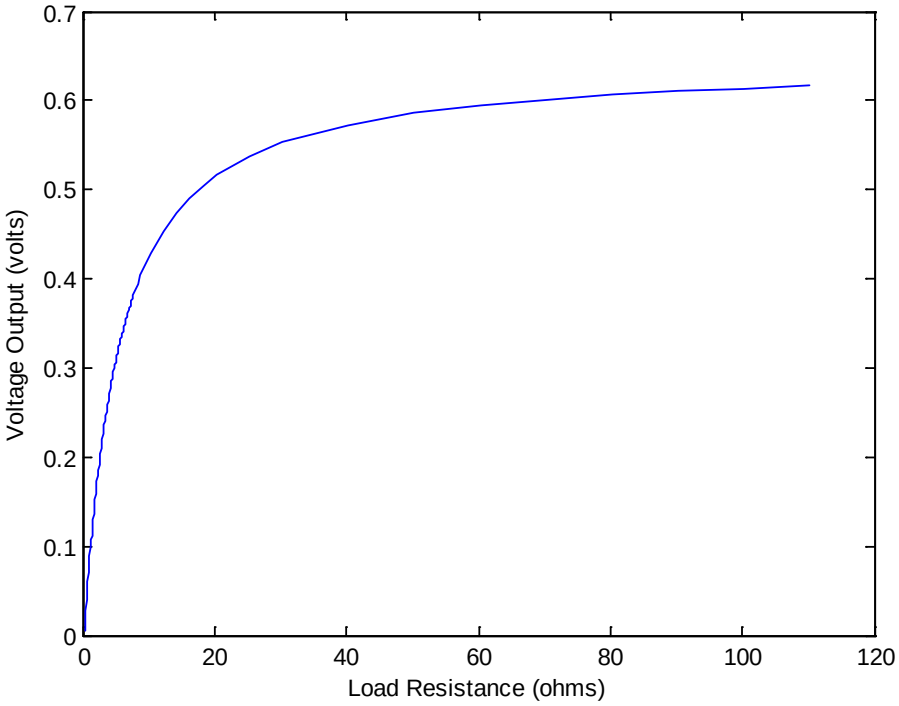

Figure 18: Voltage Output vs. Load Resistance for Loaded Test 2

The output power versus load resistance curves are shown in Figure 19 for the first loaded test and in Figure 20 for the second loaded test. For the first loaded test, the power output peaks when the load resistance is around 5.8 Ω. For the second loaded test, the power output peaks when the load resistance is between 5.5 Ω and 6.8 Ω. The power output was predicted to peak when the load resistance equaled the source resistance (3.44 Ω), but the data from the loaded tests demonstrates this was not true in this case. This is most likely due to the internal resistance of the system (aside from the source resistance and the load resistance), such as that from the connecting wires, making the actual load resistance different than dictated by the applied load.

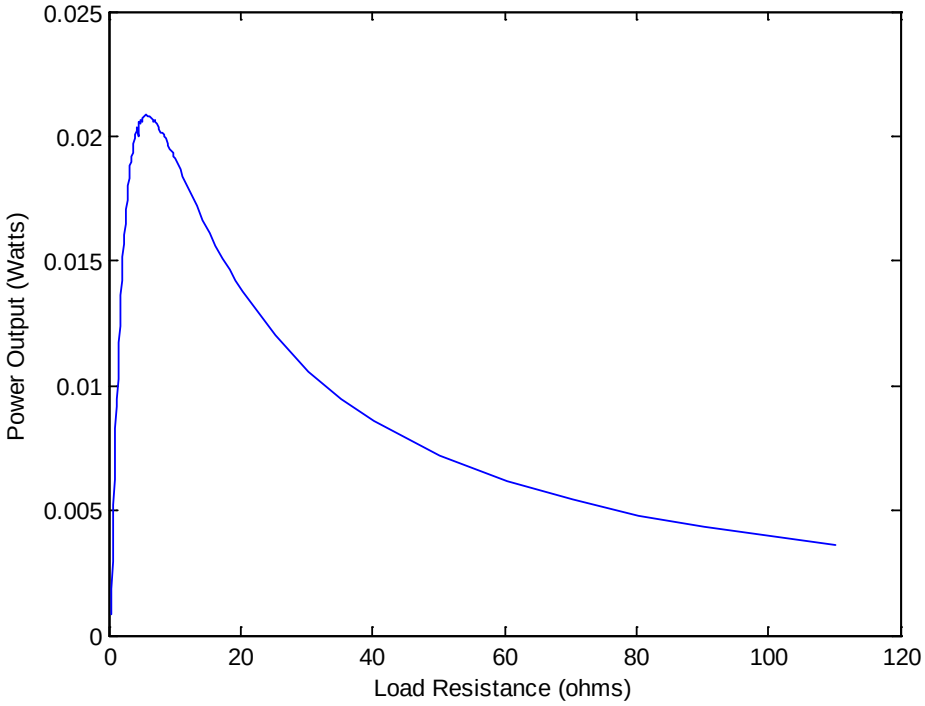

Figure 19: Power Output vs. Load Resistance for Loaded Test 1

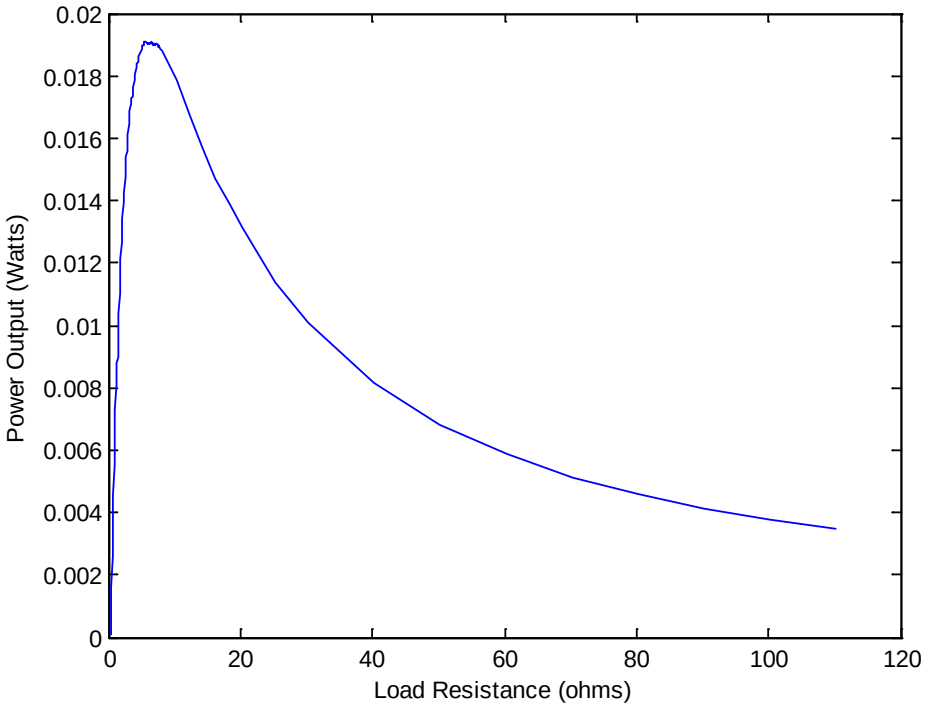

Figure 20: Power Output vs. Load Resistance for Loaded Test 2

The output power versus output voltage curves are shown in Figure 21 for the first loaded test and in Figure 22 for the second loaded test. For the first loaded test, the power output peaks when the voltage output is between 0.3480 V and 0.3510 V. For the second loaded test, the power output peaks when the voltage output is between 0.3240 V and 0.3600 V.

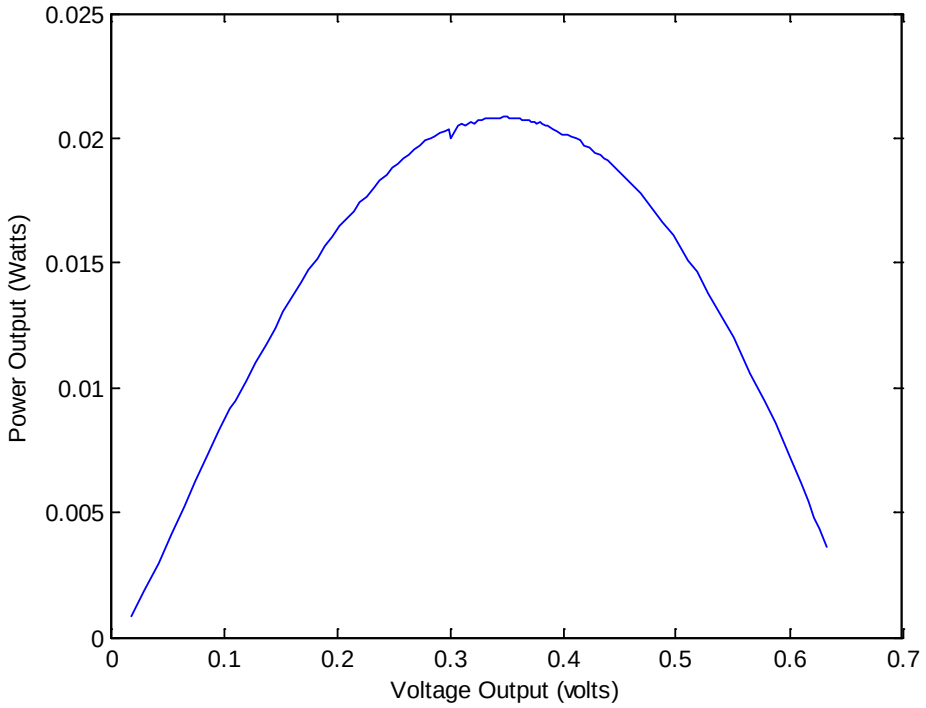

Figure 21: Power Output vs. Voltage Output for Loaded Test 1

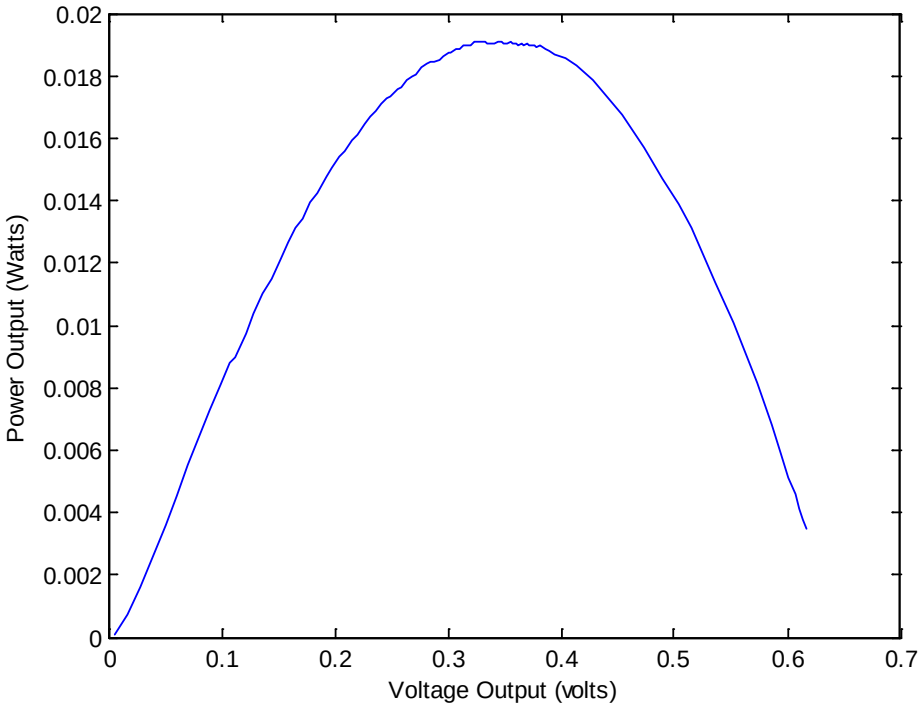

Figure 22: Power Output vs. Voltage Output for Loaded Test 2

The output voltage versus current curves are shown in Figure 23 for the first loaded test and Figure 24 for the second loaded test. These curves were expected to be nearly linear, but the data deviates from linearity as it begins to curl back underneath itself around 0.085 amps for the first loaded test and 0.08 amps for the second loaded test.

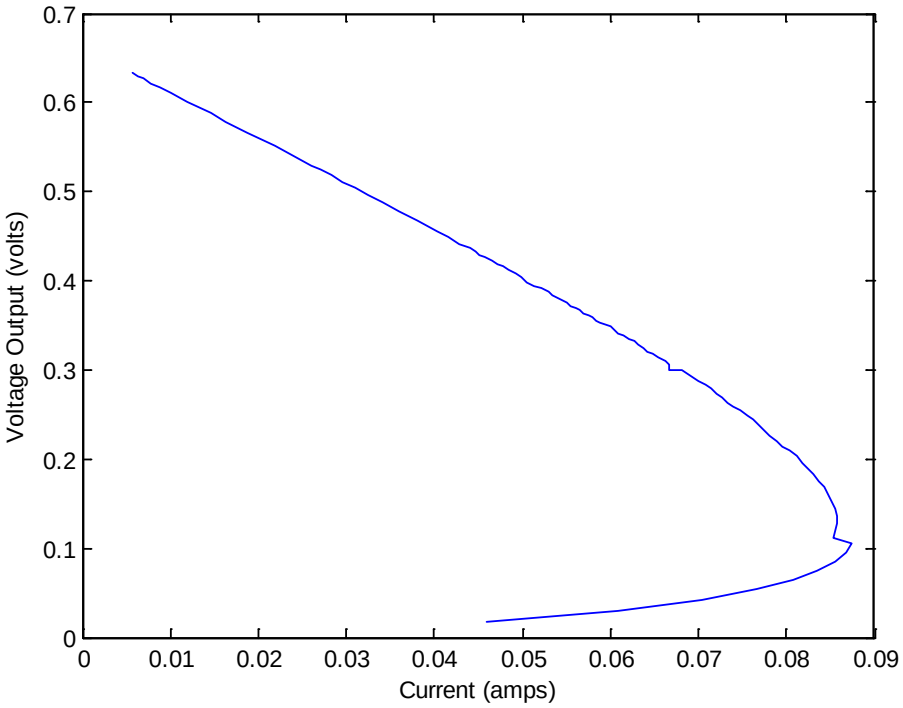

Figure 23: Voltage Output vs. Current for Loaded Test 1

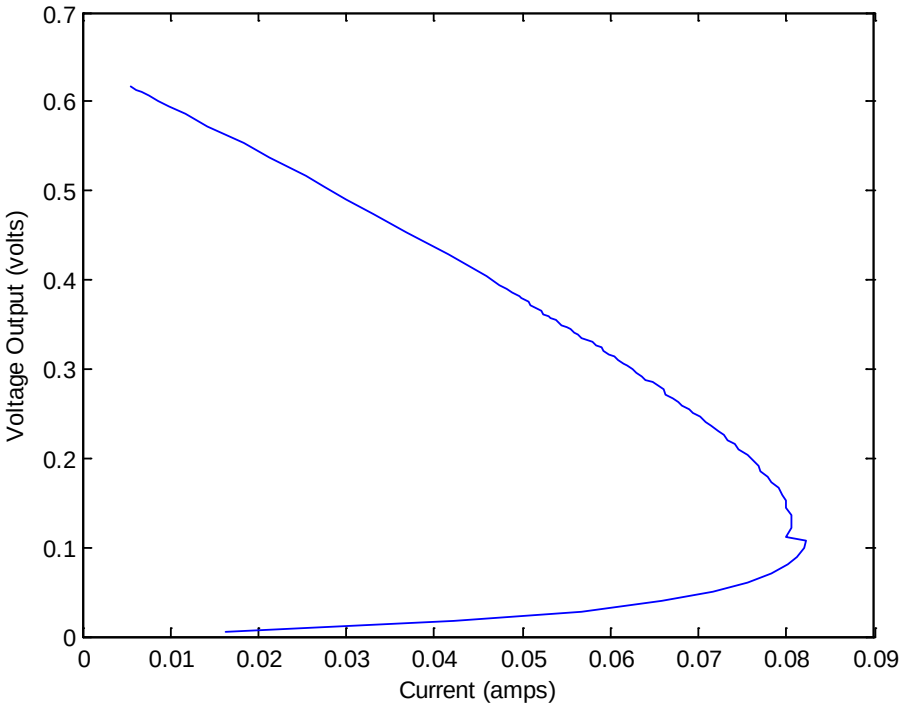

Figure 24: Votlage Output vs. Current for Loaded Test 2

The output power versus current curves are shown in Figure 25 for the first loaded test and Figure 26 for the second loaded test. These curves were expected to be nearly parabolic, but the data deviates from a parabolic curve and curls back underneath itself.

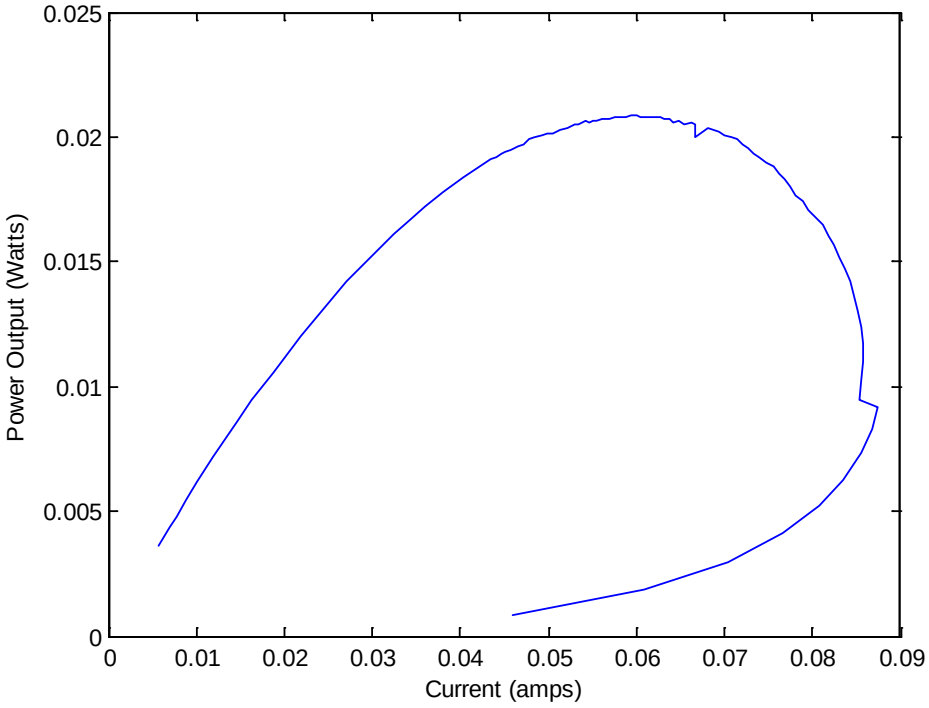

Figure 25: Power Output vs. Current for Loaded Test 1

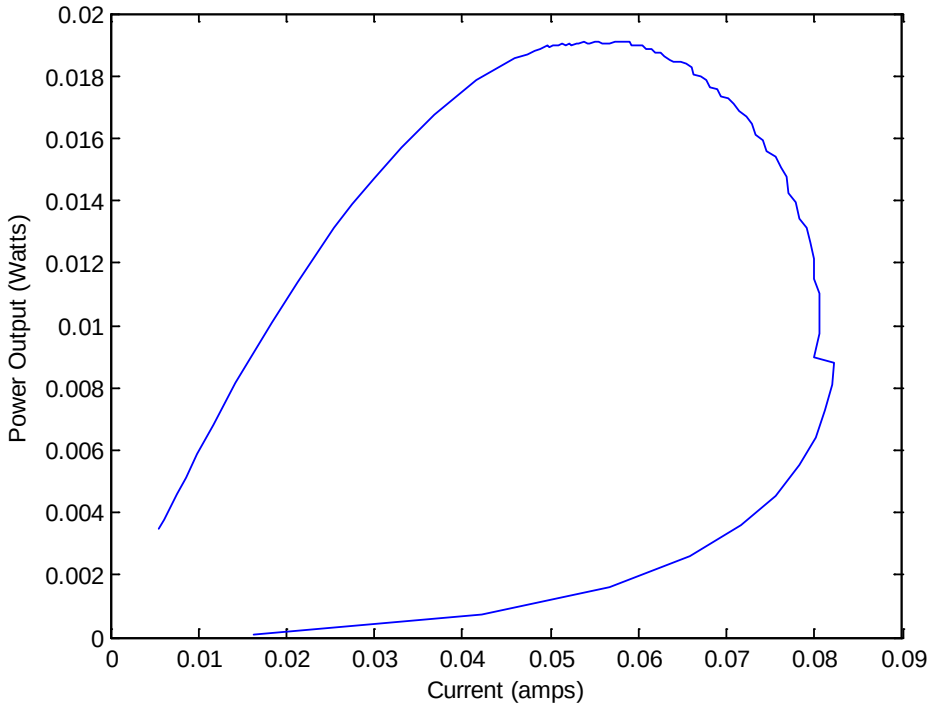

Figure 26: Power Output vs. Current for Loaded Test 2

The deviation from linearity in the voltage-current characteristics and the deviation from a parabolic curve in the power-current characteristics can be explained by the dependency of the temperature gradient on the current [2]. This phenomenon, known as Joule heating, describes the heat produced in a semiconductor (or conductor) when a current is passed through it [6]; because the current causes an increase in the material's temperature, the temperature gradient is not constant. If the temperature gradient was not dependent on the current (and thus constant), the relationship between the voltage and the current would be linear, and the relationship between the power output and the current would be parabolic [2].

Conclusions and Future Recommendations

As demonstrated in the indoor open circuit test, the steady-state open circuit voltage was not maintained. The thermoelectric module allowed too much heat to flow through it to maintain the steady-state temperature gradient, consequently increasing the temperature of the heat sink and decreasing the temperature gradient. This ultimately caused the open-circuit voltage produced by the module to decrease. In order to avoid this problem and increase the STEG efficiency, the heat sink needs further capability to dissipate heat since its own mass was not enough. This could be achieved through a finned heat sink or a heat sink with water cooling.

A study at MIT reached a peak STEG efficiency of 5.2% in a vacuum but only about 0.5% when operating in air, both cases without optical concentration [2]. This system's efficiency is an order of magnitude lower than that reached by MIT without a vacuum, peaking around 0.03%. In order to match or exceed the 0.5% efficiency in air, this system would need design improvements. The aforementioned theoretical design analysis assumed better conditions than were met, including a 179^{o}C temperature gradient (the actual temperature gradient was measured to be around 15^{o}C). If this experiment were to be completed again, the theoretical analysis should be reassessed with more realistic operating conditions, producing a new and more appropriate thermal concentration ratio from which the absorber size could be calculated.

The main problem in this device was the low temperature gradient across the thermoelectric module (about 15^{o}C compared to the 179^{o}C in the original design), which could be improved through operation in a vacuum as had been assumed in the initial design. The Carnot efficiency of the thermoelectric module scales with the temperature

gradient [17]. Thus, if the theoretical design had been followed (including having an evacuated environment), this efficiency could have been improved by a factor of 10. For this experiment to be repeated and achieve significantly improved efficiency, an evacuated environment is necessary. The design of the vacuum chamber would need to be able to survive the pressure differential characteristic of a vacuum, which would require a stronger material, a thicker material, a domed material, or a combination of these for the covering.

This STEG was designed under the objective of reaching the maximum power output for the system. For maximum power output, the load resistance should equal the source resistance (although in this case, the power output did not peak when the load resistance equaled the source resistance). Yet this is not the case for maximum thermal efficiency – to achieve maximum thermal efficiency, the following equation shows the relationship between load resistance and source resistance [4]:

$$R_L = R_S\sqrt{1+ZT}$$

In order to maximize the efficiency of the system, this relationship should have been taken into account in the STEG's design.

For STEGs to enter the consumer solar energy market and be competitive with photovoltaics, which currently dominate this market [2], STEG efficiency needs to greatly increase and at least match current efficiencies found in photovoltaic solar panels. For common crystalline silicon solar cells, efficiency is standardly 12% [18]. Considering that MIT's peak efficiency was measured at 5.2% [2] and only 0.03% for this research, room for major improvements exists before STEGs can even begin to compete.

References

1. McLamb, E. Energy's Future Today. *Ecology Global Network: Energy*. 2011 Sept. 6. <http://www.ecology.com/2011/09/06/fossil-fuels-vs-renewable-energy-resources>.
2. Kraemer, D., et al. High-performance flat-panel solar thermoelectric generators with high thermal concentration. *Nature Materials, 10,* 532-8. 2011 May 1.
3. Bergman, T. L., et al. *Introduction to Heat Transfer* (6th ed.). 2011. Jefferson City: John Wiley & Sons, Inc.
4. Angrist, S. W. *Direct Energy Conversion*. Allyn and Bacon Series in Mechanical Engineering and Applied Mechanics, ed. F. Kreith. 1965. Boston: Allyn and Bacon, Inc.
5. Mills, D. Advances in solar thermal electricity technology. *Solar Energy 76*, 19-31. 2004.
6. MacDonald, D. K. C. *Thermoelectricity: An introduction to the principles.* 1962. New York: John Wiley & Sons, Inc.
7. *Thermoelectrics*. 2013. California Institute of Technology: Materials Science. <http://thermoelectrics.caltech.edu/thermoelectrics/engineering.html>.
8. Telkes, M. The Efficiency of Thermoelectric Generators. *Journal of Applied Physics 18*, 1116-27. 1947.
9. Telkes, M. Solar Thermoelectric Generators. *Journal of Applied Physics 25*, 765-77. 1954.
10. Goldsmid, H. J. Thermoelectric Applications of Semiconductors. *Journal of Electronics and Control 1*(2), 218-22. 1955.

11. Goldsmid, H. J., et al. Solar Thermoelectric Generation Using Bismuth Telluride Alloys. *Solar Energy 24*, 435-440. 1979.

12. Rizzoni, G. *Principles and Applications of Electrical Engineering* (5th ed.). 2005. McGraw-Hill Education.

13. Kraemer, D., et al. Supplementary information: High-performance flat-panel solar thermoelectic generators with high thermal concentration. *Nature Materials 10*. 2011 May 1.

14. Scherrer, H. and S. Scherrer. *CRC Handbook of Thermoelectrics.* Ed. D. M. Rowe. 1995. Boca Raton, FL: CRC Press.

15. Window Technologies: Low-E Coatings. *Efficient Windows Collaborative*. 2012. Regents of the University of Minnesota, Twin Cities Campus, College of Design, Center for Sustainable Building Research. <http://www.efficientwindows.org/lowe.cfm>.

16. *G2-35-0315 Thermoelectric Module Specifications.* Traverse City, MI: Tellurex.

17. Moran, M. J. and H. N. Shapiro. *Fundamentals of Engineering Thermodynamics,* 6th ed. 2008. John Wiley & Sons, Inc.

18. What is the energy payback for PV? *PV FAQs*. 2004 Dec. The National Renewable Energy Laboratory for the U. S. Department of Energy.